On the Local Delay and Energy Efficiency of Clustered HetNets

Xiaojie Dong, Fu-Chun Zheng, *Senior Member, IEEE,* Xu Zhu, *Senior Member, IEEE,* and Timothy O'Farrell, *Senior Member, IEEE*

***Abstract*—Due to the dense and generally random deployment of base stations (BSs) in heterogeneous networks (HetNets), stochastic geometry has increasingly been used to analyze the performance of HetNets. Considering the geographical distribution of BSs, however, the commonly assumed Poisson point process (PPP) may not be accurate enough. In contrast, a Poisson cluster process (PCP) proves more realistic for the deployment of BSs. In this paper, by using the discontinuous transmission (DTX) mode, the local delay and energy efficiency based on PCP have been analyzed. The expressions of local delay and energy efficiency have been derived and it is found theoretically and via simulations that the local delay is larger and the energy efficiency is lower under PCP compared to PPP because of the strong intra-cluster interference. In addition, we found that the performances of PCP based HetNets are close to those of PPP for the high mute probability case and low signal-to-interference ratio (SIR) threshold case, where the impact of clustering diminishes. Moreover, the energy efficiency can be optimized further with a low local delay by jointly adjusting the mute probability and BS density within a cluster. Finally, we found that the local delay could decrease with the increase of the density of BSs by setting the proper mute probability, which is different from the PPP case.**

***Index Terms*—Poisson cluster processes (PCP), energy efficiency, local delay, random discontinuous transmission (DTX) scheme, heterogeneous networks (HetNets).**

I. Introduction

DUE to the rapid increase of wireless traffic, some data needs to be off-loaded from macrocells, and as such heterogeneous networks (HetNets) have become a powerful solution [1]. HetNets comprise a macrocell network overlaid with small cells which are served by lower power base stations (BSs), such as picocells, femtocells, remote radio heads, relays and wireless WiFi access points [2]. Deployment of small cells can improve the end-user throughput and expand macrocells' edge coverage. Nevertheless, the dense deployment of small cells can also be challenging [3].

In a wireless network, local delay is fundamentally essential for the dense deployment of small cells, which can reflect the quality of service (QoS) of the network [4]. A good QoS for a HetNet means that data is transmitted in a limited time, e.g., with several milliseconds' delay as targeted in 5G. Generally, there are mainly two kinds of delay: transmission delay and queuing delay. Transmission delay reflects the time of transmitting data successfully over the wireless link, while queuing delay reflects the time of waiting over the rest of the network. In this paper, only transmission delay is considered.

Energy efficiency is another key indicator of system performance in a wireless network [5]–[6]. Due to the explosive growth of traffic, energy consumption of wireless networks is rapidly increasing, leading to significant greenhouse gas emission. Hence, energy efficiency is one of the main issues considered in the next generation mobile communication systems (e.g. 5G). Especially, for the dense deployment of small cells, the energy efficiency is more important [7]–[8]. In this paper, energy efficiency is defined as the ratio of the average area network throughput to average area power consumption. Both local delay and energy efficiency will be dealt with in this paper.

A. Related Work and Motivations

Due to the rapidly increasing wireless traffic, the deployment of BSs in HetNets has become denser and denser, leading to the emergence of ultra dense network (UDN). On the other hand, the geographical positions of BSs in UDN are also becoming almost random. As such, stochastic geometry has emerged as a powerfully analytical tool for HetNets (or UDN).

In fact, there has been much research on Poisson point process (PPP) based HetNet' models, especially on the aspect of the energy-delay tradeoff, which is one of the four fundamental tradeoffs in green communications [9]. References [10] and [11] provided the analytical framework of the local delay, and some concrete expressions for the local delay in different cases were obtained. Moreover, in [11], local delay was analyzed in different situations, including interference only, noise only, interference and noise. The local delay in the relay network was also analyzed in [12]. The local delay was reduced by using frequency-hop multiple access technology in

Manuscript received June 20, 2018; revised December 20, 2018; accepted January 20, 2019. Date of publication ... ; date of current version December. The work of F.-C. Zheng was supported in part by a Shenzhen Municipality/HITSZ start-up grant entitled "Energy-Efficient Low-Latency Wireless Networks", the National Basic Research Program of China (973 Program) under grant 2012CB316004, and the U.K. Engineering and Physical Sciences Research Council under Grant EP/K040685/2. The associate editor coordinating the review of this paper and approving it for publication was W. Song. (Corresponding author: Fu-Chun Zheng.)

X. Dong and F.-C. Zheng are with School of Electronic and Information Engineering, Harbin Institute of Technology (Shenzhen), Shenzhen 518055, China (e-mail: 543107840@qq.com and fzheng@ieee.org).

X. Zhu is with the Department of Electrical Engineering and Electronics, University of Liverpool, Liverpool L69 3GJ, U.K. (e-mail: x-uzhu@liverpool.ac.uk).

T. O'Farrell is with Department of Electronic & Electrical Engineering, University of Sheffield, Sheffield S1 4ET, UK (e-mail: t.ofarrell@sheffield.ac.uk).

[13]. Based on the random local delay, the energy efficiency of the downlink HetNets was analyzed in [14]. In addition, the effect of coordinated transmission on local delay and energy efficiency were also analyzed in [15]. Different from the above works assuming that the users are static, the users' mobility is considered in [16] and [17]. In [16], two extreme user mobilities -static and infinite mobility- were analyzed. In [17], the analysis of local delay was extended to the case of finite user mobility. In all these existing works, the fundamental assumption is Poisson point process (PPP).

On the other hand, energy saving strategies have become very necessary for UDN. As such, random discontinuous transmission scheme (DTX) has been used to improve energy efficiency. The performance of the random DTX in mobile cellular networks was analyzed in many papers. For example, it was shown that, for a Long-Term Evolution (LTE) network, DTX can achieve much improved energy efficiency [18]–[19]. Reference [20] investigated the maximum achievable energy saving by coalescing the cell DTX with the deployment of a clean-slate network. In [21] and [23], a sleeping scheme was investigated in HetNets to improve energy efficiency by using the tools of stochastic geometry. Furthermore, energy efficiency was investigated in PPP based ultra dense HetNets in [22], without considering the random DTX scheme. In [24], the energy-spectrum tradeoff was researched in a device-to-device (D2D) based HetNet. In [25], the energy efficiency was optimized in the green coordinated multipoint (CoMP) HetNet. However, none of above papers has employed a Poisson cluster process (PCP) and the DTX scheme to study the local delay and energy efficiency.

Considering the fact that users (hence the BSs) are generally clustered in the hot spots, the above PPP assumption may not be accurate enough. In contrast, PCP can describe the scenarios where BSs are distributed as clusters, and is therefore more realistic [26]. Hence, some works have been reported in HetNet analysis based on PCP. The cumulative distribution function of the distance was derived in [27]. In [28], the distribution properties of the interference were derived and upper and lower bounds with PCP distribution were provided. A Laplace functional of the interference in heterogeneous radio access networks was derived in [29]. Moreover, a new accurate formula was derived for the probability generating function in [30]. In [31], the cumulative density function of the nearest neighbor was studied. In [32]– [36], the probability of coverage was investigated. In addition, the probability of outage and the average achievable rate were analyzed in [32] and [33]. The conclusion that PCP based model converges to PPP based model when the cluster radius tends to infinity was drawn in [34] and [35]. Nevertheless, none of these works has examined the local delay and energy efficiency in a PCP setting with different path-loss exponents. This is the motivation of this paper, which analyzes the local delay and energy efficiency with random discontinuous transmission (DTX) scheme under the PCP based HetNet model.

B. Contributions and Organizations

Characterization of Local Delay and Energy Efficiency: Using the conditional probability generating functional, the local delay and energy efficiency of PCP with DTX scheme have been derived in this paper. From the formulas, it has been found that the local delay and energy efficiency based on PCP are closely related to transmission power, density of BSs, mute probability, signal-to-interference ratio (SIR) threshold and path-loss exponent, which however are different from those of PPP. Furthermore, we analyze theoretically that the local delay is larger and energy efficiency is lower than that of PPP.

Analyses of Key Parameters: The local delay under PCP is a monotonically decreasing function with cluster radius, and the energy efficiency is an increasing function of cluster radius. In addition, the effect of BSs densities depends on the path-loss exponent, mute probability and SIR threshold. Moreover, the energy efficiency can be optimized to a maximum with a low local delay in terms of the number of within-cluster BSs.

Results of Numerical Analysis: Based on the derived expression, the local delay and energy efficiency are analyzed numerically with respect to the key system parameters such as cluster radius and mute probability. Numerical results show that, for the same density of BSs, the local delay is larger and the energy efficiency is lower under PCP than under PPP with regard to a finite radius. The local delay under PCP with a finite cluster radius will decrease with the increase of the density of BSs in some cases, which is different from that of PPP. Besides, the performance gaps between PCP and PPP are reduced in the cases of high mute probability and low SIR threshold. Finally, the numerical analyses match the simulation results within allowable error margins.

This paper is organized as follows: Section II presents the system model. In Section III, the expression of the local delay and energy efficiency are derived and the key parameters are discussed. In Section IV, we analyze the energy efficiency with respect to the key parameters. In section V, numerical and simulation results are discussed. Finally, conclusion is provided in Section VI.

II. System Model

A. Heterogeneous Networks Model

We model a static HetNet with K independent network tiers, and denote $\mathcal{K} = \{1, 2, ..., K\}$. The locations of BSs satisfy Neyman-Scott cluster point processes [38], which is a special Poisson cluster process (PCP) with homogeneous independent cluster centres. A Neyman-Scott cluster point process consists of parent points and daughter points. The parent points form the cluster centers, while the daughter points are independently distributed within the clusters. Especially, if the daughter points follow uniform distribution in a ball of cluster radius R, the Neyman-Scott cluster point processes is also termed Matern cluster process (MCP), which is adopted as the PCP model in this paper. The density function $f(x_d)$ of the daughter points in a cluster under MCP is given by [28]

$$f(x_d) = \begin{cases} \dfrac{1}{\pi R^2}, & \|x_d\| \le R \\ 0, & otherwise \end{cases}, \tag{1}$$

where $\|x_d\|$ is the distance between the daughter point in a cluster and the center of the cluster.

In this paper, the parent points form a homogeneous independent Poisson process with density $\lambda_{p,i}$, and the number of daughter points in a cluster follows poisson distribution with mean $\bar{c}_i$ in the ith tier. The density of ith tier is $\lambda_i = \lambda_{p,i}\bar{c}_i$, which implies the parent points are not included. Meanwhile, the transmission power and the path-loss exponents are respectively P_i and α_i ($\alpha_i > 2$). The set of BSs in the ith tier is Φ_i, so the set of overall BSs is denoted by $\Phi = \bigcup_{i\in\mathcal{K}} \Phi_i$.

In Fig. 1, we show the two-tier HetNets under PPP and under PCP respectively with the DTX scheme, where the gray points represent the mute BSs while the red points and the blue points, respectively, represent active macro cells and active pico cells. Pico cells under PPP are distributed independently of one another, but pico cells under PCP are clustered. Through the comparison between PPP and PCP, PCP should normally be more realistic for the deployment of BSs, due to the fact that users are generally clustered in the hot spots.

Assume that a typical mobile user is located at origin $o \in R^2$ and the location of the BS in ith tier is x_i. In particular, the BS in the ith tier offering the strongest average received signal strength (RSS) is located at $x_{i,0}$. We adopt the general path loss model, $l(x) = \|x\|^{-\alpha}$, between a BS located at x and a typical user located at origin, where $\|x\|$ is the distance between a BS and a user. Furthermore, we adopt the assumption that the power fading coefficients h_x are spatially and temporally i.i.d. Rayleigh fading with unit mean. Considering the tractability of the model, we ignore the effect of shadow fading (which does not alter much the trend of the SINR distribution (e.g. [39])). Finally, this paper neglects the noise because the density of BSs in HetNets is so high that interference is the main problem.

The strongest average RSS is considered as the association criterion in this paper[1]. Assuming that a kth-tier BS is associated with the user, this index of the serving BS is expressed by

$$k = \arg\max_{i\in\mathcal{K}} P_i\|x_{i,0}\|^{-\alpha_i}, \tag{2}$$

where the power fading coefficient is averaged out in the long term.

In this paper, the random discontinuous transmission (DTX) mode [18] is adopted at the BS. Assume that time is divided into discrete slots, and the BS transmits the data packets only if it becomes active (serving at least one user [41]). The ith-tier BS then transmits the data packets with the probability of $1-\zeta_i$ in each slot, i.e., it keeps mute with the probability of $\zeta_i \in [0,1)$. Let $\Phi_{i,t}$ denote the set of active BSs in the time slot t in the ith tier and the aggregate interference can be expressed as:

$$I_{\Phi\setminus\{x_{k,0}\},t} = \sum_{i\in\mathcal{K}} \sum_{x_i\in\Phi_i\setminus\{x_{k,0}\}} P_i h_x \|x_i\|^{-\alpha_i} \mathcal{I}(x_i \in \Phi_{i,t}), \tag{3}$$

where $\mathcal{I}(\cdot)$ is the indicator function. That is, if the $x_i \in \Phi_{i,t}$, BSs are active and $\mathcal{I} = 1$. Otherwise, $\mathcal{I} = 0$. The received SIR of the typical mobile user in the time slot t is

$$\mathrm{SIR}_{k,t} = \frac{P_k h_x \|x_{k,0}\|^{-\alpha_k}}{I_{\Phi\setminus\{x_{k,0}\},t}}. \tag{4}$$

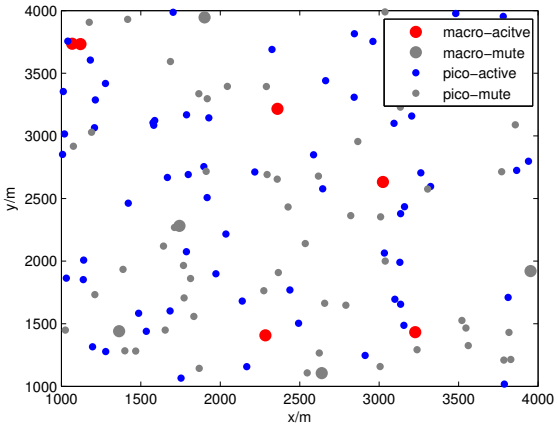

(a) PPP

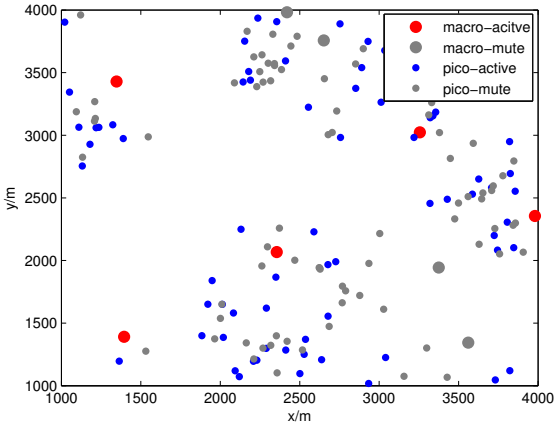

(b) PCP

Fig. 1: A two-tier HetNet with (a) PPP and (b) PCP respectively. Density of parent process in the *1*st tier is $\lambda_{p,1} = 1/(\pi 500^2)$ cells/m^2, and $\bar{c}_1$ = 1. Density of parent process in the 2nd tier is $\lambda_{p,2} = 2\lambda_{p,1}$, and $\bar{c}_2$ = 5. PPP has the same density of BSs as PCP.

B. Performance Metrics

Inspired by [14], this paper considers two main performance metrics: local delay and energy efficiency.

Local Delay: This paper considers the case where a transmission will not stop until the successful reception of a data packet at the mobile user. Therefore, the distribution of the number of time slots for a successful transmission conditioned

[1]Note that an RSS bias can also be introduced here to realize range expansion (RE), which can be an effective means to increase the coverage of small cells and to off-load some traffic from the macro cells [39]. Similar to range expansion, the densely deployed clustered small cells in this paper can be regarded as another coverage expansion technique for small cells (i.e. there would always be one or more "favourable" small cell(s) offering better RSS for most users anyway). On the other hand, the potentially larger interference suffered by off-loaded users in the bias based RE schemes may compromise the gain of off-loading. Such a trade-off is certainly an interesting point for further research.

on Φ is geometrical. The probability of a successful transmission denoted by $\mathcal{C}_\Phi$ conditioned on r and Φ is given by

$$\mathbb{P}(\mathcal{C}_\Phi) = (1-\zeta_k)\mathbb{P}(\text{SIR}_{k,t} > \theta \mid r, \Phi), \tag{5}$$

where θ is the SIR threshold, r is the distance between the user and the associated BS, and $1-\zeta_k$ means that only when the associated BS is active, can the data packet be transmitted. A successful transmission happens when the received SIR at the user is larger than the SIR threshold θ. The mean number of time slots for a successful transmission conditioned on r and Φ is proportional to $Pr(\mathcal{C}_\Phi)^{-1}$. The local delay is defined as the mean number of time slots for a successful transmission. When the user is associated with the kth tier, the local delay can be defined as

$$D_k = \mathbb{E}_{r,\Phi}[\frac{1}{\mathbb{P}(\mathcal{C}_\Phi)}]. \tag{6}$$

According to the law of total probability, the average local delay can be written by

$$D = \sum_{k\in\mathcal{K}} \mathcal{A}_k D_k, \tag{7}$$

where $\mathcal{A}_k$ is the probability that the typical user is associated with the BS in the kth tier.

Energy Efficiency: In this paper, the network energy efficiency is defined as the ratio of average area network throughout to average area power consumption. The network throughput [14] is given by

$$\tau = D^{-1}\log(1+\theta)\sum_{i=1}^{K}(1-\zeta_i)\lambda_{p,i}\bar{c}_i, \tag{8}$$

where $\log(1+\theta)$ is the rate of data packet transmitted successfully with unit nats/s/Hz. From (8), network throughput means that the average number of successfully transmitted nats per second per hertz per unit area.

On the other hand, to examine the network energy efficiency, a linear power consumption model [37] is adopted for the BS. The power consumption of the kth-tier BS is

$$P = \begin{cases} P_{i,a} + \Delta_i P_i, & if \quad P_i > 0 \\ P_{i,m}, & if \quad P_i = 0 \end{cases}, \tag{9}$$

where $P_{i,a}$ is the static power of the active BS, and $P_{i,m}$ is the static power of the muted BS in the ith tier. Δ_i is the slope of power consumption in the ith tier. Hence, the energy efficiency [14], with unit nats/J/Hz, is given by

$$\begin{aligned}\eta_{\text{EE}} &= \frac{\tau}{P_{area}} \\ &= \frac{D^{-1}\log(1+\theta)\sum_{i=1}^{K}(1-\zeta_i)\lambda_{p,i}\bar{c}_i}{\sum_{i=1}^{K}\lambda_{p,i}\bar{c}_i[(1-\zeta_i)(P_{i,a}+\Delta_i P_i)+\zeta_i P_{i,m}]}.\end{aligned} \tag{10}$$

III. Local Delay

This section will explore characteristics of the local delay with respect to key system parameters.

A. General Case and Main Results

Based on the aforementioned definitions, we have the following results about local delay.

Theorem 1: The local delay with a random DTX scheme in a K-tier PCP distributed HetNet is given by

$$\begin{aligned}D = &\sum_{k=1}^{K}\int_0^\infty \frac{2\pi\lambda_k}{1-\zeta_k}\exp\left\{-\pi\sum_{i=1}^{K} r^{\frac{2\alpha_k}{\alpha_i}}\lambda_i(\frac{P_i}{P_k})^{\frac{2}{\alpha_i}} - \right. \\ &\left.\sum_{i=1}^{K}\lambda_{p,i}\int_{R^2}[1-\exp(-\bar{c}_i\beta_i(y))]dy\right\}\times \\ &\int_{R^2}\exp(-\bar{c}_k\beta_k(y))f(y)dyrdr,\end{aligned} \tag{11}$$

where

$$\beta_i(y) = (1-\zeta_i)\int_{R^2}\frac{-f(x)}{\|x-y\|^{\alpha_i}/sP_i+\zeta_i}dx. \tag{12}$$

Proof: See Appendix A.

The density function $f(\cdot)$ of the daughter points is given in (1). The expression in Theorem 1 can accurately describe the properties of the local delay in a K-tier PCP distributed HetNet. However, as the local delay in (11) is not a closed form, it is discommodious to analyze the local delay and energy efficiency with respect to the key system parameters. Therefore, for analysis of the local delay and energy efficiency under PCP, an approximate but closed-form expression is obtained, which is shown below.

Corollary 1: The local delay with a random DTX scheme in a K-tier PCP distributed HetNet can be approximated as

$$\begin{aligned}D = &\sum_{k=1}^{K}\int_0^\infty \frac{2\pi\lambda_k}{1-\zeta_k}\exp\{-\pi\sum_{i=1}^{K} r^{\frac{2\alpha_k}{\alpha_i}}\lambda_i(\frac{P_i}{P_k})^{\frac{2}{\alpha_i}} + \\ &\pi\sum_{i=1}^{K}\lambda_i(1-\zeta_i)r^{\frac{2\alpha_k}{\alpha_i}}(\frac{P_i}{P_k})^{\frac{2}{\alpha_i}}\mathcal{Z}(\theta,\zeta_i,\alpha_i) \\ &+\frac{\bar{c}_k(1-\zeta_k)r^2}{R_k^2}\mathcal{Z}(\theta,\zeta_k,\alpha_k)\}rdr,\end{aligned} \tag{13}$$

where

$$\mathcal{Z}(\theta,\zeta_i,\alpha_i) = \int_1^\infty \frac{\theta}{\theta\zeta_i + t^{\frac{\alpha_i}{2}}}dt. \tag{14}$$

Proof: See Appendix B.

The expression of the local delay in (13) is more tractable than the expression in (11). We can use the local delay expression in (13) to verify that the local delay under PCP is larger than that of PPP. With the increase of R_k, the local delay in (13) decreases gradually. When cluster radius R_k is infinite, the local delay reaches the minimum value, which is the same as that under PPP [14]. Affected by the local delay, from (10), the energy efficiency is lower than that of PPP for same the key system parameters.

Moreover, the local delay expression in (13) can be further simplified in some special cases. First, if we assume that BSs in all tiers have the same path-loss exponent $\{\alpha_i\} = \alpha$, Corollary 1 can be simplified into Corollary 2 below.

Corollary 2: Assuming $\{\alpha_i\} = \alpha$, the local delay can be expressed as:

$$D = \begin{cases} \sum_{k=1}^{K} \frac{\pi\lambda_k}{1-\zeta_k} \frac{1}{T^{(k)}} & T^{(k)} > 0 \\ \infty & T^{(k)} \leq 0 \end{cases}, \tag{15}$$

where

$$\begin{aligned} T^{(k)} &= T_1^{(k)} + T_2^{(k)} + T_3^{(k)}, \\ T_1^{(k)} &= \pi \sum_{i=1}^{K} \lambda_i (\frac{P_i}{P_k})^{\frac{2}{\alpha}}, \\ T_2^{(k)} &= -\pi \sum_{i=1}^{K} \lambda_i (1-\zeta_i)(\frac{P_i}{P_k})^{\frac{2}{\alpha}} \mathcal{Z}(\theta, \zeta_i, \alpha), \\ T_3^{(k)} &= -\frac{\overline{c}_k(1-\zeta_k)}{R_k^2} \mathcal{Z}(\theta, \zeta_k, \alpha). \end{aligned}$$

The above result is obtained simply by letting the path-loss exponent $\{\alpha_i\} = \alpha$ and using the equation $\int_0^\infty 2re^{-Ar^2}dr = 1/A$. ■

In this case, BSs of HetNets have the same path loss for the same transmission distance. Also, due to the disappearance of the integral of distance, the analysis of local delay is now more concise. We will use the expression in (15) for the following analysis to gain insights.

B. Effect of Cluster Radius

The BSs are assumed to satisfy PCP and the cluster radius R is a key parameter. From (15), the local delay is a monotonically decreasing function with the cluster radius R_k. Thus, two extreme cases, e.g. $R \to 0$ and $R \to \infty$, will now be discussed.

$T_3^{(k)}$ in (15) will tend to negative infinity if the cluster radius R_k tends to zero, and then the local delay tends to infinity, which is consistent with the actual situation. The clusters would become a point with all intra-BSs located at the same point, leading to an infinite interference, and the time for a successful transmission of course becomes infinity. Also, the large number of BSs within a cluster, though providing high data rates, may make the local delay large, leading to a low throughput. However, when the cluster radius R_k tends to infinity, $T_3^{(k)}$ in (15) tends to zero. We can find that the local delay in (15) will be almost invariable with the cluster radius R_k, if $R_k > R_{0,k}$, where $R_{0,k}$ is the cluster radius of saturation, making $T_3^{(k)}$ negligible.

C. Effect of Mute Probability

In this section, we will investigate the effect of the mute probability on the local delay.

Corollary 3: Letting the mute probability $\{\zeta_i\} = \zeta$, and the path-loss exponent $\{\alpha_i\} = \alpha$, $T^{(k)}$ in (15) can be expressed as

$$T^{(k)} = \frac{\pi}{(1-\zeta)D_p} \sum_{i=1}^{K} \lambda_i (\frac{P_i}{P_k})^{\frac{2}{\alpha}} - \frac{c_k(1-\zeta)}{R_k^2} \mathcal{Z}(\theta, \zeta, \alpha), \tag{16}$$

where D_p is the local delay of PPP based HetNets [14]. This results from (15) directly by letting the mute probabilities of all tiers be identical. ■

The local delay D_p of PPP based HetNets tends to infinity when the mute probability ζ approaches zero [14]. Therefore, from (16), $T^{(k)}$ will become $-\mathcal{Z}(\theta, 0, \alpha)c_k/R_k^2$, which is less than zero when $\zeta \to 0$. As a result, there is an infinite local delay under PCP based HetNets. In addition, we have $(1-\zeta)D_p = 1$ for $\zeta = 1$ [14]. Hence, $T^{(k)}$ in (16) will become a finite value $\pi \sum_{i=1}^{K} \lambda_i (P_i/P_k)^{2/\alpha}$. Thus, from (15), the local delay reaches infinity. Therefore, using the random DTX scheme, which can avoid the large local delay, in clustered HetNets is essential. Furthermore, the local delay D will become D_p for the infinite cluster radius. Affected by the local delay, the energy efficiency is the same as that of PPP. The results indirectly reveal that PCP will degenerate to PPP when the cluster radius tends to infinity [34].

D. Effect of Parent-Points Density

Fixing the average number $\overline{c}_k$ of intra-cluster BSs, we analyze the impact of the density of parent points $\lambda_{p,k}$. For a HetNet, it is crucial to study whether increasing the BS density will decrease the local delay.

Proposition 1: For the same mute probability $\{\zeta_k\} = \zeta$ and the same path-loss exponent $\{\alpha_k\} = \alpha$, the local delay is a monotonically decreasing function with $\lambda_{p,k}$, if $\overline{c}_k$ satisfies

$$\overline{c}_k < \frac{\sum_{j=1, j\neq k}^{K} \overline{c}_j (\frac{T^{(k)}}{T^{(j)}})^2 \lambda_{p,j} (\frac{\partial T_1^{(j)}}{\partial \lambda_{p,k}} + \frac{\partial T_2^{(j)}}{\partial \lambda_{p,k}})}{\sum_{j=1, j\neq k}^{K} \lambda_{p,j} (\frac{\partial T_1^{(k)}}{\partial \lambda_{p,j}} + \frac{\partial T_2^{(k)}}{\partial \lambda_{p,j}}) + T_3^{(k)}}. \tag{17}$$

Proof: See Appendix C.

From (17), whether the local delay decreases with the increase of BS parent-point density in the kth tier depends upon $\overline{c}_k$. It indicates that we can adjust $\overline{c}_k$ to make the derivative of local delay negative, so that the local delay will decrease with the increase of cluster numbers $\lambda_{p,k}$, which is beneficial for the scenario of more hotspots. When the cluster radius R_k tends to infinity, the derivative of the local delay becomes zero, and the local delay will become unrelated to $\lambda_{p,k}$ and c_k. The reason is that as the cluster radius R_k increases, the effect of the cluster decreases gradually.

E. Effect of Daughter-Points Density

We now analyze the local delay D with respect to the average number (i.e. $\overline{c}_k$) of daughter points in a cluster by fixing $\lambda_{p,k}$.

Proposition 2: For the same mute probability $\{\zeta_k\} = \zeta$ and the same path-loss exponent $\{\alpha_k\} = \alpha$, the local delay is a monotonically decreasing function with $\overline{c}_k$, if $\lambda_{p,k}$ satisfy

$$\lambda_{p,k} < \frac{\sum_{j=1, j\neq k}^{K} \lambda_{p,j} (\frac{T^{(k)}}{T^{(j)}})^2 \overline{c}_j (\frac{\partial T_1^{(j)}}{\partial \overline{c}_k} + \frac{\partial T_2^{(j)}}{\partial \overline{c}_k} + \frac{\partial T_3^{(j)}}{\partial \overline{c}_k})}{\sum_{j=1, j\neq k}^{K} \overline{c}_j (\frac{\partial T_1^{(k)}}{\partial \overline{c}_j} + \frac{\partial T_2^{(k)}}{\partial \overline{c}_j})}. \tag{18}$$

Proof: The derivative of the local delay in (15) with respect to $\overline{c}_k$ is given by

$$\frac{\partial D}{\partial \bar{c}_k} = \sum_{j=1}^{K} \frac{\partial D}{\partial T^{(j)}} \frac{\partial T^{(j)}}{\partial \bar{c}_k} + \frac{\pi \lambda_{p,k}}{1-\zeta_k} \frac{1}{T^{(k)}}, \tag{19}$$

where $\frac{\partial D}{\partial T^{(j)}}$ is calculated from Appendix C, and is invariably less than zero. $\frac{\partial T^{(j)}}{\partial \bar{c}_k}$ can be calculated as

$$\frac{\partial T^{(j)}}{\partial \bar{c}_k} = \frac{\partial T_1^{(j)}}{\partial \bar{c}_k} + \frac{\partial T_2^{(j)}}{\partial \bar{c}_k} + \frac{\partial T_3^{(j)}}{\partial \bar{c}_k}, \tag{20}$$

where

$$\begin{aligned}
\frac{\partial T_1^{(j)}}{\partial \bar{c}_k} &= \pi \lambda_{p,k} (\frac{P_k}{P_j})^{\frac{2}{\alpha}} \\
\frac{\partial T_2^{(j)}}{\partial \bar{c}_k} &= -\pi \lambda_{p,k} (1-\zeta_k) (\frac{P_k}{P_j})^{\frac{2}{\alpha}} \mathcal{Z}(\theta, \zeta_k, \alpha) \\
\frac{\partial T_3^{(j)}}{\partial \bar{c}_k} &= -\frac{(1-\zeta_k)}{R_k^2} \mathcal{Z}(\theta, \zeta_k, \alpha) \; for \; j = k.
\end{aligned}$$

$\frac{\partial D}{\partial \bar{c}_k}$ can therefore be simplified as

$$\begin{aligned}
\frac{\partial D}{\partial \bar{c}_k} = &- \sum_{j=1, j\neq k}^{K} \frac{\pi \lambda_{p,j}}{1-\zeta_j} \frac{\bar{c}_j}{T^{(j)2}} (\frac{\partial T_1^{(j)}}{\partial \bar{c}_k} + \frac{\partial T_2^{(j)}}{\partial \bar{c}_k} + \frac{\partial T_3^{(j)}}{\partial \bar{c}_k}) + \\
&\frac{\pi \lambda_{p,k}}{1-\zeta_k} \frac{1}{T^{(k)2}} [T_1^{(k)} + T_2^{(k)} - \bar{c}_k (\frac{\partial T_1^{(k)}}{\partial \bar{c}_k} + \frac{\partial T_2^{(k)}}{\partial \bar{c}_k})].
\end{aligned} \tag{21}$$

By letting $\{\zeta_k\} = \zeta$ and considering that $\partial D / \partial \bar{c}_k$ in (21) is less than zero, Proposition 2 can be proved. ■

The local delay will decrease with the increase of daughter-points density if the parent points density in the kth tier satisfies (18). Therefore, via (17) and (18), we can jointly regulate $\lambda_{p,k}$ and $\bar{c}_k$ (e.g. to make the local delay decrease with the increase of $\lambda_{p,k}$ and $\bar{c}_k$). That is when the intra-cluster interference is large, we can decrease $\lambda_{p,k}$ to reduce the inter-cluster interference, and vice versa.

F. Effect of SIR Threshold

From (14), the derivative of $\mathcal{Z}(\theta, \zeta_i, \alpha_i)$ with respect to θ can be calculated as:

$$\frac{\partial \mathcal{Z}(\theta, \zeta_i, \alpha_i)}{\partial \theta} = \int_1^{\infty} \frac{t^{\frac{\alpha_i}{2}}}{(\theta \zeta_i + t^{\frac{\alpha_i}{2}})^2} dt, \tag{22}$$

which is nonnegative.

Hence, $\mathcal{Z}(\theta, \zeta_i, \alpha_i)$ is a monotonically increasing function with the SIR threshold θ. From (15), we can observe that the local delay is a monotonically increasing function with $\theta > 0$. Therefore, with the increase of the data rate, the local delay will increase, which implies that the actual network throughput is also subject to the local delay. As a result, there exists an optimization problem of network throughput with respect to the SIR threshold. The result agrees with the definition of the network throughput in (8).

IV. Energy Efficiency

In this section, we will discuss the energy efficiency in HetNets. With the local delay derived in (15), the energy efficiency can be analyzed from (10).

A. Effect of Parent-Point Density

Note that the local delay is related to the density of BSs, therefore, the energy efficiency can be expressed as

$$\eta_{\text{EE}} = \frac{1}{D} \cdot \eta(\lambda_{p,k}), \tag{23}$$

where

$$\eta(\lambda_{p,k}) = \frac{\log(1+\theta) \sum_{i=1}^{K} (1-\zeta_i) \lambda_{p,i} \bar{c}_i}{\sum_{i=1}^{K} \lambda_{p,i} \bar{c}_i [(1-\zeta_i)(P_{i,a} + \Delta_i P_i) + \zeta_i P_{i,m}]}. \tag{24}$$

Then, the derivative of the energy efficiency with respect to density of parent points can be divided into two parts:

$$\frac{\partial \eta_{\text{EE}}}{\partial \lambda_{p,k}} = \frac{\partial \eta_{\text{EE}}}{\partial D} \frac{\partial D}{\partial \lambda_{p,k}} + \frac{1}{D} \frac{\partial \eta(\lambda_{p,k})}{\partial \lambda_{p,k}}, \tag{25}$$

where $\frac{\partial \eta_{\text{EE}}}{\partial D}$ can be calculated as $-\frac{1}{D}\eta_{\text{EE}}$ according to (10), which is invariably less than zero, and $\frac{\partial D}{\partial \lambda_{p,k}}$ has been obtained from Appendix C. Hence, energy efficiency will be a monotonically increasing function with $\lambda_{p,k}$ if $\frac{\partial D}{\partial \lambda_{p,k}}$ is less than zero and $\frac{\partial \eta(\lambda_{p,k})}{\partial \lambda_{p,k}}$ is larger than zero, which implies

$$\begin{cases} \frac{\pi \bar{c}_k}{1-\zeta_k} \frac{1}{T^{(k)}} < -\sum_{j=1}^{K} \frac{\partial D}{\partial T^{(j)}} \frac{\partial T^{(j)}}{\partial \lambda_{p,k}} \\ P_{k,ave} < \frac{(1-\zeta_k) \sum_{i=1, i\neq k}^{K} P_{i,ave} \lambda_i}{\sum_{i=1, i\neq k}^{K} (1-\zeta_i) \lambda_i} \end{cases}, \tag{26}$$

where $P_{i,ave} \triangleq (1-\zeta)(P_{k,a} + \Delta_k P_k) + \zeta P_{k,m}$ for $k \in \mathcal{K}$ [14].

From (26), the average number of BSs within a cluster and the transmission power have an effect on the derivative of energy efficiency, which reveals whether the energy efficiency increase with parent-point density increase will depend on the transmission power and the property of the local delay, given the mute probability. The first condition means that the local delay decreases with the increase of $\lambda_{p,k}$. If $\bar{c}_k$ can be adjusted to meet the first condition, the energy efficiency will then depend on the kth-tier BS transmission power.

B. Effect of Daughter-Point Density

We now investigate the energy efficiency with respect to $\bar{c}_k$ by fixing $\lambda_{p,k}$. The derivative of energy efficiency with respect to $\bar{c}_k$ is expressed by

$$\frac{\partial \eta_{\text{EE}}}{\partial \bar{c}_k} = \frac{\partial \eta_{\text{EE}}}{\partial D} \frac{\partial D}{\partial \bar{c}_k} + \frac{1}{D} \frac{\partial \eta(\bar{c}_k)}{\partial \bar{c}_k}, \tag{27}$$

where $\eta(\bar{c}_k) = \eta(\lambda_{p,k})$. Therefore, if $\frac{\partial D}{\partial \bar{c}_k}$ is negative and $\frac{\partial \eta(\bar{c}_k)}{\partial \bar{c}_k}$ is positive, energy efficiency will be a monotonically increasing function with $\bar{c}_k$. For a sufficiently large cluster radius, we have

$$\begin{cases} \frac{\pi \lambda_{p,k}}{1-\zeta_k} \frac{1}{T^{(k)}} < -\sum_{j=1}^{K} \frac{\partial D}{\partial T^{(j)}} \frac{\partial T^{(j)}}{\partial \bar{c}_k} \\ P_{k,ave} < \frac{(1-\zeta_k) \sum_{i=1, i\neq k}^{K} P_{i,ave} \lambda_i}{\sum_{i=1, i\neq k}^{K} (1-\zeta_i) \lambda_i} \end{cases}. \tag{28}$$

According to the local delay analysis with respect to $\bar{c}_k$, the first condition in (28) can be met by adjusting $\lambda_{p,k}$. Therefore, we only consider the second condition in (28) to see whether increasing the average number of BSs in a cluster in the kth tier to improve the energy efficiency will only depend upon the kth-tier transmission power, given the same mute probability ζ. Moreover, the energy efficiency of the kth tier will become zero since there is no base station in the kth tier when $\bar{c}_k \to 0$. Nevertheless, when $\bar{c}_k \to \infty$, the energy efficiency becomes very low due to the extremely large intra-cluster interference. Hence, there exists an optimal $\bar{c}_k$ to maximize the energy efficiency with a finite local delay.

The conclusions in (26) and (28) can be used in many systems, e.g. ultra dense HetNets: the high BS density can improve the energy efficiency.

C. Effect of SIR Threshold

Due to $\eta_{\text{EE}}(\theta|_{\theta=0}) = \eta_{\text{EE}}(\theta|_{\theta=\theta_c}) = 0$, there exists an optimal SIR threshold θ, which maximises the energy efficiency [14]. From (22), the local delay is a monotonically increasing function with θ, therefore, the reciprocal of local delay is a monotonically decreasing function. Moreover, as the energy efficiency is related to the local delay D and the transmission rate $\log(1+\theta)$, we consider a simplified equation $\eta(\theta) = D^{-1}\log(1+\theta)$, which is equivalent to $\eta_{\text{EE}}(\theta)$. By letting $\frac{\partial \eta(\theta)}{\partial \theta} = 0$, the optimal SIR threshold θ^* can be obtained by

$$\frac{D(\theta|_{\theta=\theta^*})}{D^{'}(\theta|_{\theta=\theta^*})} = (1+\theta^*)\log(1+\theta^*), \tag{29}$$

where $D^{'}$ is the derivative of the local delay with respect to θ. In fact, $x\log(x)$ is an increasing function of x, $\forall x > 1$. Consequently, the larger $D(\theta|_{\theta=\theta^*})/D^{'}(\theta|_{\theta=\theta^*})$, the larger the optimal SIR threshold θ^*. Also, from (29), the optimal SIR threshold θ^* is related to the mute probability, density of BSs and path-loss exponent due to the local delay D. Therefore, the key system parameters can be adjusted to satisfy (29), so as to achieve a targeted data rate with maximum energy efficiency.

V. Numerical and Simulation Results

In this section, we carry out numerical analyses of the local delay and energy efficiency to verify and complement the aforementioned analysis. For easy comparison between PCP and PPP, the same denotations as in [14] are adopted. A two-tier HetNet structure, consisting of macro cells (tier 1) and pico cells (tier 2), is used. The practical deployment of macro cells is usually unicellular clustered, and therefore, let $\bar{c}_1 = 1$. In addition, in the following discussion, the radius generally refers to the radius R_2 of pico cell clusters. Also, the related parameters are $P_1 = 20W$, $P_2 = 0.13W$, $P_{1,a} = 130W$, $P_{2,a} = 6.8W$, $\Delta_1 = 4.7$, and $\Delta_2 = 4.0$ [37]. The values of BS density are according to References [39] and [40]. Simulations are also carried out to verify the theoretical/numerical results. For all the simulations, unless stated otherwise, we chose a 20km x 20km area to deploy macro cells and pico cells, which are two independent PCPs.

A. Effect of Mute Probability

In Fig. 2, the local delay as a function of mute probability is shown, where $\lambda_{p,1}=1/(\pi 500^2)$ cells/m^2, $\lambda_{p,2}=5\lambda_{p,1}$, $\bar{c}_1$=1, $\bar{c}_2$=5, α=4, R_1=600m, ∞, R_2=800m, ∞. The local delay of infinity on the left is because the mute probability ζ is so small that there are many active BSs, leading to large interference among BSs, and the associated BS can hardly successfully transmit data to the typical user. The tendency to infinity on the right is because the mute probability ζ is so large that there is almost no active BS, which increases the association distance. In addition, for the same SIR threshold θ, the mute probability ζ under PCP spans a smaller range with respect to the limited local delay. The reason is that BSs are located within the clusters under PCP and the intra-cluster interference becomes much larger and dominant compared with the PPP model. As a result, existence of clusters transforms the structure of the interference.

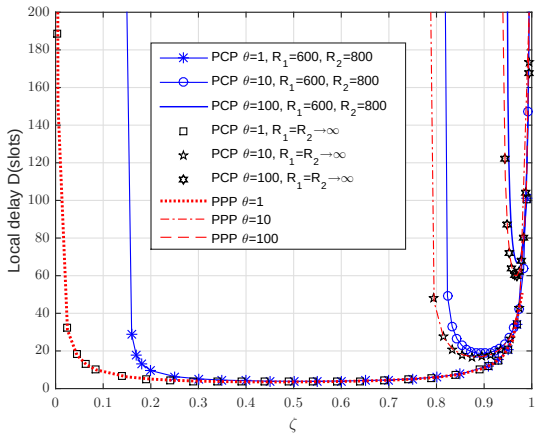

Fig. 2: The local delay as a function of mute probability, where $\lambda_{p,1}=1/(\pi 500^2)$ cells/m^2, $\lambda_{p,2}=5\lambda_{p,1}$, $\bar{c}_1$=1, $\bar{c}_2$=5, α=4, R_1=600m, ∞, R_2=800m, ∞.

When the cluster radii tend to infinity, the local delays under PCP and those under PPP become very similar. It suggests that the increasing radii make the local delay under PCP approximately equal to the local delay under PPP. The property of clustering weakens gradually with the increase of the radii, and as a result, the distributions of PCP and PPP become very similar [34]. In addition, the high mute probability can make up the gap between the local delays of PCP and PPP no matter what the radii are.

B. Effect of Cluster

In Fig. 3, we show the local delay as a function of cluster radius R_2, where $\lambda_{p,1}=1/(\pi 500^2)$ cells/m^2, $\lambda_{p,2}=5/(\pi 500^2)$ cells/m^2, $\bar{c}_1$=1, $\bar{c}_2$=5, α=4, θ=1, R_1=2000m. Let the radius of macro cells tend to infinity, then we observe the effect of the radius of pico cells on local delay. Both numerical and simulation results are plotted, which match each very well. When the cluster radius R_2 is small enough, the local

delay tends to infinity. The reason is that BSs in a cluster are located within a very small area, leading to a large intra-interference among BSs, and the data packet is unlikely to be successfully transmitted. As the radius R_2 increases, the intra-cluster interference becomes lower, and finally, the local delay converges to a constant value. Furthermore, if the mute probability ζ increases, the critical radius R_c will decrease, where $R_c \triangleq \inf\{R_2 : D(R_2) < \infty\}$. The reason is that when the high mute probability is adopted in BS, the number of active BSs is small, and then the intra-interference is also relatively small.

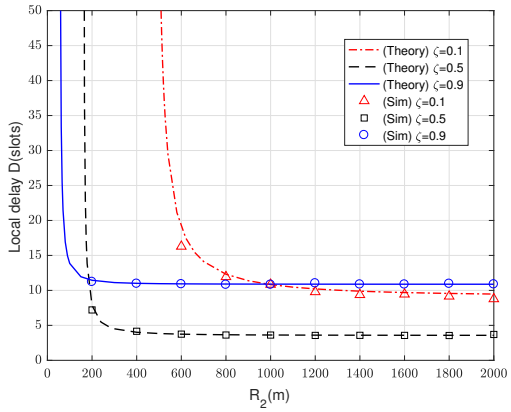

Fig. 3: Local delay as a function of cluster radius R_2, where $\lambda_{p,1}$=1/(π500^2) cells/m^2, $\lambda_{p,2}$=5/(π500^2) cells/m^2, $\bar{c}_1$=1, $\bar{c}_2$=5, α=4, θ=1, R_1=2000m.

In Fig. 4, local delay and energy efficiency with respect to 2nd-tier daughter density $\bar{c}_k$ are shown, where $\lambda_{p,1}$=1/(π500^2) cells/m^2, $\lambda_{p,2}$=4/(π500^2) cells/m^2, $\bar{c}_1$=1, α=4, θ=1, ζ_1=0.2, R_1=1000m, R_2=500m. Both numerical and simulation results are plotted and they match each other well. We can observe that there exists a minimum local delay in terms of $\bar{c}_2$ when $\zeta_2 = 0.2$. With the increase of the mute probability of picocells, the local delay will converge to a certain value with respect to the number of within-cluster picocells. This is because the effects of the association distance and the intra-cluster interference cancel each other out. Nevertheless, the energy efficiency will increases with respect to the number of within-cluster picocells. Therefore, we can increase $\bar{c}_2$ to improve the energy efficiency without increasing the local delay. Furthermore, when the mute probability $\zeta_2 = 0.5$, the energy efficiency shows the best performance. The reason is that there exists a large interference when the mute probability is low and the association distance increases when the mute probability is high. Hence, by adjusting within-cluster density $\bar{c}_k$ and the mute probability ζ_k, the performances of the local delay and energy efficiency of PCP based HetNets can both improve to a large extent.

C. Effect of Density

In Fig. 5, the local delay and energy efficiency as a function of mute probability with different densities of parent points in a two-tier HetNet are shown, where $\lambda_{p,1}$=1/(π500^2) cells/m^2, $\lambda_{p,2}$=1.25, 2.5, 3.75/(π500^2) cells/m^2, $\bar{c}_1$=1, $\bar{c}_2$=4, α=4, θ=1, R_1=700m, R_2=800m, ζ_1=0.5. For the same density, the local delay under PCP is larger and the energy efficiency under PCP is lower. This is because the interference under PCP is larger than that under PPP due to clustering. Moreover, in the PCP network, the local delay is related to transmission power and density of BSs, even though $\{\zeta_k\} = \zeta$. Therefore, in Fig. 5, local delays for PCP are different when $\zeta_1 = \zeta_2 = 0.5$.

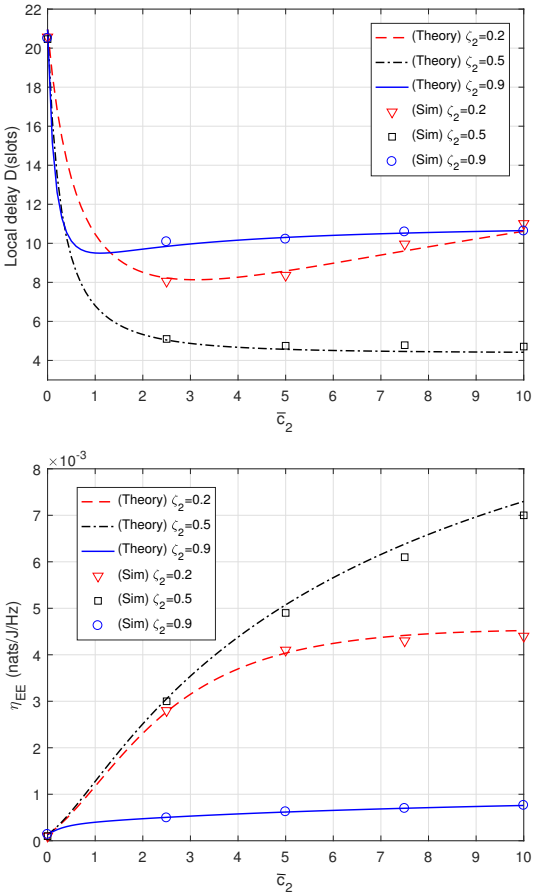

Fig. 4: Local delay and energy efficiency with respect to 2nd-tier daughter density in a two-tier HetNet, where $\lambda_{p,1}$=1/(π500^2) cells/m^2, $\lambda_{p,2}$=4/(π500^2) cells/m^2, $\bar{c}_1$=1, α=4, θ=1, ζ_1=0.2, R_1=1000m, R_2=500m.

In a PCP, for a given cluster radius $R_2 < \infty$, if we increase the density of 2nd-tier clusters, not only will the interference increase, but also the distance between the user and the associated BS will decrease. The decrease of local delay with the increase of the density of 2nd-tier clusters is because the decrease of association distance becomes dominating factor. On the other hand, in a PPP, the local delay increases with the increase of the density of BSs in the 2nd tier, because the interference is the dominating factor. Also, the gap between local delays of PCP and PPP will decrease with the density of 2nd-tier clusters. Thus, when analyzing the local delay, we can use PPP to model the locations of BSs in a high density

network, e.g. UDN. The high mute probability destroying the cluster role can also reduce the energy efficiency gap between PCP and PPP, namely, energy efficiency can be analyzed based on PPP in a high mute probability network. Moreover, there exists an optimal mute probability ζ_2 to maximize the energy efficiency η_{EE} both under a PCP and under a PPP.

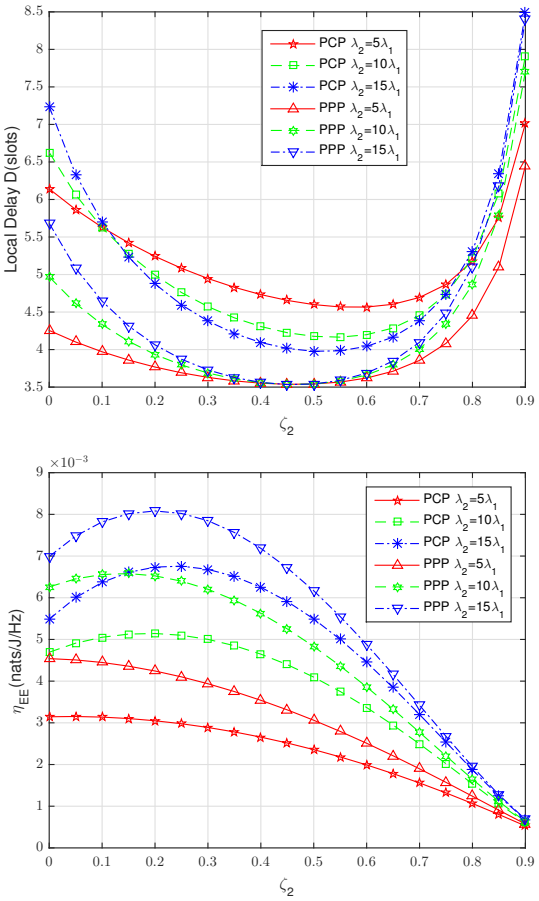

Fig. 5: Local delay and energy efficiency as a function of mute probability with different densities of parent process in a two-tier HetNet, where $\lambda_{p,1}$=1/(π500^2) cells/m^2, $\lambda_{p,2}$=1.25, 2.5, 3.75/(π500^2) cells/m^2, $\bar{c}_1$=1, $\bar{c}_2$=4, α=4, θ=1, R_1=700m, R_2=800m, ζ_1=0.5.

D. Effect of SIR Threshold

In Fig. 6, the local delay and energy efficiency with respect to SIR threshold and mute probability in a two-tier HetNet are shown, where $\lambda_{p,1}$=1/(π500^2) cells/m^2, $\lambda_{p,2}$=5/(π500^2) cells/m^2, $\bar{c}_1$=1, $\bar{c}_2$=5, λ_2=25λ_1, α=3.5, R_1=600m, R_2=800m. With the increase of the SIR threshold θ, the local delay gradually approaches infinity, and the energy efficiency increases at first and then decreases, which verifies the properties of local delay and energy efficiency on the SIR threshold in (22) and (29). For the small SIR threshold θ, the probability of the received SIR being above the SIR threshold is large,

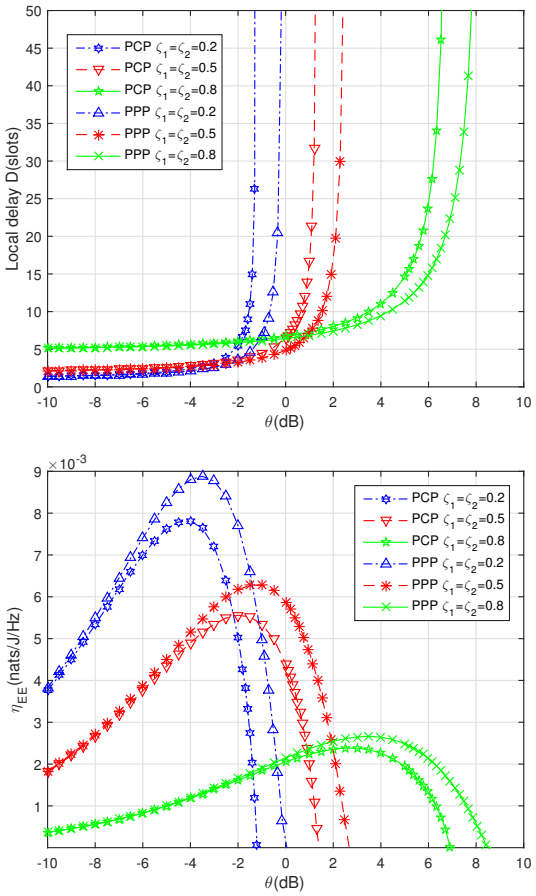

Fig. 6: Local delay and energy efficiency with respect to SIR threshold and mute probability in a two-tier HetNet, where $\lambda_{p,1}$=1/(π500^2) cells/m^2, $\lambda_{p,2}$=5/(π500^2) cells/m^2, $\bar{c}_1$=1, $\bar{c}_2$=5, λ_2=25λ_1, α=3.5, R_1=600m, R_2=800m.

therefore the local delay is small. However, due to the small SIR threshold θ, the transmission rate is low, leading to the low energy efficiency. On the other hand, for the large SIR threshold θ, the low energy efficiency is mainly caused by the large local delay.

In addition, the increase of the mute probability ζ causes the increase of both the critical SIR threshold θ_c, where $\theta_c \triangleq \sup\{\theta : D(\theta) < \infty\}$ and the optimal SIR threshold θ^* that maximizes the energy efficiency. The reason is that the higher mute probability implies the lower number of active BSs. On the one hand, fewer interfering BSs results in the limited local delay for a high SIR threshold; on the other hand, the serving BS maintains low active time, leading to a lower energy efficiency.

The critical SIR threshold θ_c of PCP shows little difference from that of PPP under diverse mute probability. Affected by the above critical SIR threshold θ_c, the optimal SIR threshold θ^* under PCP in terms of the energy efficiency has little difference from that of PPP. Moreover, the PCP shows nearly the same properties as PPP on local delay and energy efficiency for the low SIR threshold θ. The reason is that the low SIR threshold makes the interference have less impact,

reducing the effect of clustering. In this case, PPP is certainly applicable to modeling the BS locations.

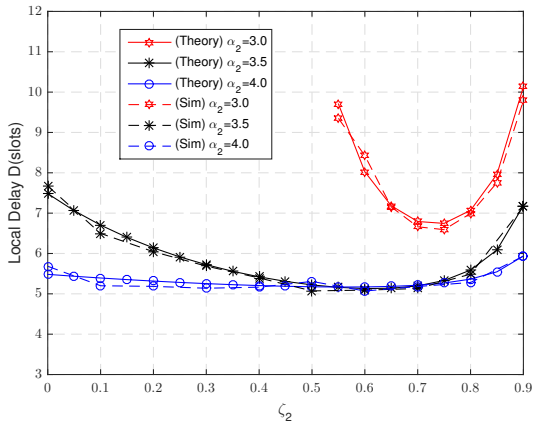

Fig. 7: Local delay D as a function of mute probability with different path-loss exponents, where $\lambda_{p,1}$=1/(π500^2) cells/m^2, $\lambda_{p,2}$=2/(π500^2) cells/m^2, $\bar{c}_1$=1, $\bar{c}_2$=4, α_1=3.5, θ=1, R_1=2000m, R_2=800m.

E. Effect of Path loss exponent

The path loss exponent α_i has a significant effect on the interference among BSs, therefore, we analyzed the local delay with respect to α.

Macro cells and pico cells have different path-loss exponents. Therefore, in Fig. 7, we now fix the path-loss exponent of macro cells $\alpha_1 = 3.5$, and let the path-loss exponent of pico cells $\alpha_2 = 3, 3.5, 4$ respectively. With the increase of path-loss exponent, the local delay decreases, because the received signal at the typical user is more severely affected by the interfering BSs for the smaller path-loss exponent α_2. In addition, if $\alpha_2 < \alpha_1$, the local delay will be infinity for a small mute probability, which further implies that a DTX scheme is essential for a good network performance. The reason is that pico cells are dense, leading to massive BS interference in this case. In addition, to verify Corollary 1 and the theoretical analysis, the corresponding Monte Carlo simulation results are also shown in Fig. 7. The simulation results of the local delay (dashed curves) clearly match the numerical results well.

VI. Conclusion

In this paper, the local delay and energy efficiency of HetNets with DTX scheme based on PCP have been derived. The expressions demonstrated that the local delay and energy efficiency under the PCP are related to transmission power, cluster radii and BS density apart from the mute probability, path-loss exponent and SIR threshold. Hence, the key parameters were examined in terms of the local delay and energy efficiency. Moreover, numerical results and theoretical analysis showed that the local delay is larger and the energy efficiency is lower under PCP than under PPP with respect to the same key system parameters. In addition, a suitable number of BSs within a cluster can maximize the energy efficiency with a low local delay. The local delay under PCP with a finite cluster radius will decrease with the increase of the BS density in some cases. Furthermore, the PPP can replace the PCP to model BSs for the high mute probability case and low SIR threshold case. Finally, the simulation results have well verified the validity of the expressions of the local delay and energy efficiency.

Appendix A
Proof of Theorem 1

Proof: The probability of a successful transmission with the random discontinuous transmission (DTX) mode conditioned on Φ is expressed as

$$\begin{aligned}
&\mathbb{P}(\mathcal{C}_\Phi)\\
&= (1-\zeta_k)\mathbb{P}(\mathrm{SIR}_{k,t} > \theta|\Phi)\\
&\overset{a}{=} (1-\zeta_k)\mathbb{P}(\frac{P_k h_x \|x_{k,0}\|^{-\alpha_k}}{I_{\Phi\setminus\{x_{k,0}\},t}} > \theta|\Phi)\\
&\overset{b}{=} (1-\zeta_k)\mathbb{E}_{I_{\Phi\setminus\{x_{k,0}\},t}}[\exp(-\frac{\theta I_{\Phi\setminus\{x_{k,0}\},t}}{P_k\|x_{k,0}\|^{-\alpha_k}})|\Phi]\\
&\overset{c}{=} (1-\zeta_k)\prod_{i\in\mathcal{K}}\prod_{x_i\in\Phi_i\setminus\{x_{k,0}\}}(\frac{1-\zeta_i}{1+sP_i\|x_i\|^{-\alpha_i}}+\zeta_i),
\end{aligned} \tag{30}$$

where $s = \frac{\theta}{P_k\|x_{k,0}\|^{-\alpha_k}}$. Also (a) is from the SIR in (4); (b) is due to the power fading coefficients following an exponent i.i.d. distribution with unit mean; (c) follows the Laplace transform of $I_{x_i} = P_i h_x \|x_i\|^{-\alpha_i}\mathcal{I}(x_i \in \Phi_i)$.

The conditional local delay given r can be calculated as

$$\begin{aligned}
&D_k(r)\\
&= \mathbb{E}_\Phi\left[\frac{1}{\mathbb{P}(\mathcal{C}_\Phi)}\right]\\
&= \frac{1}{(1-\zeta_k)}\prod_{i\in\mathcal{K},i\neq k}\mathbb{E}\left[\prod_{x_i\in\Phi_i}\frac{1+sP_i\|x_i\|^{-\alpha_i}}{1+s\zeta_iP_i\|x_i\|^{-\alpha_i}}\right]\times\\
&\qquad\mathbb{E}^!_x\left[\prod_{x_k\in\Phi_k}\frac{1+sP_k\|x_k\|^{-\alpha_k}}{1+s\zeta_kP_k\|x_k\|^{-\alpha_k}}\right].
\end{aligned} \tag{31}$$

Using the conditional probability generating functional of PCP, the conditional local delay can be evaluated as

$$\begin{aligned}
&D_k(r)\\
&= \frac{1}{(1-\zeta_k)}\prod_{i=1}^{K}\underbrace{\exp(-\lambda_{p,i}\int_{R^2}[1-\exp(-\bar{c}_i\beta_i(y))]dy)}_{\text{Term 1}}\\
&\quad\times\underbrace{\int_{R^2}\exp(-\bar{c}_k\beta_k(y))f(y)dy}_{\text{Term 2}},
\end{aligned} \tag{32}$$

where

$$\beta_i(y) = (1-\zeta_i)\int_{R^2}\frac{-f(x)}{\|x-y\|^{\alpha_i}/sP_i+\zeta_i}dx. \tag{33}$$

Based on the association rule of the strongest received signal strength, the probability distribution function [33] of the distance r between the user and its associated BS is

$$f(r) = \frac{2\pi\lambda_k}{\mathcal{A}_k}\exp[-\pi\sum_{i=1}^{K}\lambda_i(\frac{P_i}{P_k})^{\frac{2}{\alpha_i}}r^{\frac{2\alpha_k}{\alpha_i}}]r. \quad (34)$$

So the average local delay in the kth tier can be expressed as

$$D_k = \int_0^\infty D_k(r)f(r)dr. \quad (35)$$

According to the law of total probability in (7), the local delay in (11) can be determined. ■

APPENDIX B
PROOF OF COROLLARY 1

Proof: In (32), the first term of $D_k(r)$ can be simplified as follows

$$\begin{aligned}
&\exp(-\sum_{i=1}^{K}\lambda_{p,i}\int_{R^2}[1-\exp(-\bar{c}_i\beta_i(y))]dy)\\
&\overset{a}{\geq}\exp(-\sum_{i=1}^{K}\lambda_{p,i}\int_{R^2}\bar{c}_i\beta_i(y)dy)\\
&\overset{b}{=}\exp(-\sum_{i=1}^{K}\lambda_i(1-\zeta_i)\int_{R^2}\int_{R^2}\frac{-f(x)}{\|x-y\|^{\alpha_i}/sP_i+\zeta_i}dxdy)\\
&\overset{c}{\approx}\exp(2\pi\sum_{i=1}^{K}\lambda_i(1-\zeta_i)\int_{d_i}^{\infty}\frac{1}{y^{\alpha_i}/sP_i+\zeta_i}ydy)\\
&\overset{d}{=}\exp(\pi\sum_{i=1}^{K}\lambda_i(1-\zeta_i)r^{\frac{2\alpha_k}{\alpha_i}}(\frac{P_i}{P_k})^{\frac{2}{\alpha_i}}\mathcal{Z}(\theta,\zeta_i,\alpha_i)),
\end{aligned} \quad (36)$$

where (a) is from the fact that $1-\exp(-x)\leq x$; (b) is from $\beta_i(y)$ in (33); (c) is the variable transformation and follows the change of the coordination from rectangular coordinate system to polar coordinate system and $d_i = (\frac{P_i}{P_k})^{\frac{1}{\alpha_i}}r^{\frac{\alpha_k}{\alpha_i}}$; (d) is also the variable transformation with $t = y^2r^{-\frac{2\alpha_k}{\alpha_i}}(\frac{P_k}{P_i})^{\frac{2}{\alpha_i}}$ and $\mathcal{Z}(\theta,\zeta_i,\alpha_i)=\int_1^\infty\frac{\theta}{\theta\zeta_i+t^{\frac{\alpha_i}{2}}}dt$.

The second term of $D_k(r)$ has an approximate expression as

$$\begin{aligned}
&\int_{R^2}\exp(-\bar{c}_k\beta_k(y))f(y)dy\\
&\quad\overset{a}{\geq}\exp(\int_{R^2}\int_{R^2}\frac{\bar{c}_k(1-\zeta_k)\theta\|y\|^{-\alpha_k}}{\theta\zeta_k\|y\|^{-\alpha_k}+r^{-\alpha_k}}f(x)f(y-x)dy)\\
&\quad\overset{b}{=}\exp(\bar{c}_k(1-\zeta_k)\int_{R^2}\frac{\theta\|y\|^{-\alpha_k}}{\theta\zeta_k\|y\|^{-\alpha_k}+r^{-\alpha_k}}(f*f)(y)dy)\\
&\quad\overset{c}{\approx}\exp(\frac{2\bar{c}_k(1-\zeta_k)}{R_k^2}\int_r^\infty\frac{\theta y^{-\alpha_k}}{\theta\zeta_k y^{-\alpha_k}+r^{-\alpha_k}}ydy)\\
&\quad\overset{d}{=}\exp(\frac{\bar{c}_k(1-\zeta_k)r^2}{R_k^2}\mathcal{Z}(\theta,\zeta_k,\alpha_k)),
\end{aligned} \quad (37)$$

where (a) follows the change of variables; (b) is obtained from the definition of convolution; (c) results from the change of the coordinates from rectangular to polar coordinate system; (d) is also the variable transformation with $t = y^2r^{-\frac{2\alpha_k}{\alpha_i}}(\frac{P_k}{P_i})^{\frac{2}{\alpha_i}}$.

$D_k(r)$ can be obtained by using (36) and (37) and then the local delay in (13) can be calculated according to Appendix A.

■

APPENDIX C
PROOF OF PROPOSITION 1

Proof: The derivative of the local delay in (15) with respect to $\lambda_{p,k}$ is given as

$$\frac{\partial D}{\partial\lambda_{p,k}} = \sum_{j=1}^{K}\frac{\partial D}{\partial T^{(j)}}\frac{\partial T^{(j)}}{\partial\lambda_{p,k}} + \frac{\pi\bar{c}_k}{1-\zeta_k}\frac{1}{T^{(k)}}, \quad (38)$$

where $\frac{\partial D}{\partial T^{(j)}}$ can be calculated as

$$\frac{\partial D}{\partial T^{(j)}} = -\frac{\pi\lambda_j}{1-\zeta_j}\frac{1}{T^{(j)2}}. \quad (39)$$

From (39), $\frac{\partial D}{\partial T^{(j)}}$ is always negative, therefore only $\frac{\partial T^{(j)}}{\partial\lambda_{p,k}}$ needs to be analyzed, which is expressed by

$$\frac{\partial T^{(j)}}{\partial\lambda_{p,k}} = \frac{\partial T_1^{(j)}}{\partial\lambda_{p,k}} + \frac{\partial T_2^{(j)}}{\partial\lambda_{p,k}}, \quad (40)$$

where

$$\begin{aligned}
\frac{\partial T_1^{(j)}}{\partial\lambda_{p,k}} &= \pi\bar{c}_k(\frac{P_k}{P_j})^{\frac{2}{\alpha}}\\
\frac{\partial T_2^{(j)}}{\partial\lambda_{p,k}} &= -\pi\bar{c}_k(1-\zeta_k)(\frac{P_k}{P_j})^{\frac{2}{\alpha}}\mathcal{Z}(\theta,\zeta_k,\alpha)\\
\frac{\partial T_3^{(j)}}{\partial\lambda_{p,k}} &= 0.
\end{aligned}$$

So the derivative of local delay is given as

$$\frac{\partial D}{\partial\lambda_{p,k}} = -\sum_{j=1}^{K}\frac{\pi\lambda_j}{1-\zeta_j}\frac{1}{T^{(j)2}}(\frac{\partial T_1^{(j)}}{\partial\lambda_{p,k}}+\frac{\partial T_2^{(j)}}{\partial\lambda_{p,k}}) + \frac{\pi\bar{c}_k}{1-\zeta_k}\frac{1}{T^{(k)}}. \quad (41)$$

Considering $T_1^{(k)} = \sum_{i=1}^{K}\lambda_{p,i}\frac{\partial T_1^{(k)}}{\partial\lambda_{p,i}}$ and $T_2^{(k)} = \sum_{i=1}^{K}\lambda_{p,i}\frac{\partial T_2^{(k)}}{\partial\lambda_{p,i}}$, $\frac{\partial D}{\partial\lambda_{p,k}}$ can transform into

$$\begin{aligned}
\frac{\partial D}{\partial\lambda_{p,k}} =& -\sum_{j=1,j\neq k}^{K}\frac{\pi\bar{c}_j}{1-\zeta_j}\frac{1}{T^{(j)2}}\lambda_{p,j}(\frac{\partial T_1^{(j)}}{\partial\lambda_{p,k}}+\frac{\partial T_2^{(j)}}{\partial\lambda_{p,k}})+\\
&\frac{\pi\bar{c}_k}{1-\zeta_k}\frac{1}{T^{(k)2}}[\sum_{j=1,j\neq k}^{K}\lambda_{p,j}(\frac{\partial T_1^{(k)}}{\partial\lambda_{p,j}}+\frac{\partial T_2^{(k)}}{\partial\lambda_{p,j}})+T_3^{(k)}].
\end{aligned} \quad (42)$$

Letting $\{\zeta_k\}=\zeta$, Proposition 1 can be proved. ■

REFERENCES

[1] D. Liu, Y. Chen, K. K. Chai, T. Zhang and M. Elkashlan, "Two-dimensional optimization on user association and green energy allocation for HetNets with hybrid energy sources", *IEEE Trans. Commun.*, vol. 63, no. 11, pp. 4111-4124, Nov. 2015.

[2] M. Kamel, W. Hamouda and A. Youssef, "Ultra-dense networks: A survey", *IEEE Commun. Surveys Tuts.*, vol. 18, no. 4, pp. 2522-2545, 2016.

[3] D. Lopez-Perez et al., "Enhanced intercell interference coordination challenges in heterogeneous networks," *IEEE Wireless Commun. Mag.*, vol. 18, no. 3, pp. 22-30, Jun. 2011.

[4] J. G. Andrews et al., "Rethinking information theory for mobile ad hoc networks," *IEEE Commun. Mag.*, vol. 46, no. 12, pp. 94-101, Dec. 2008.

[5] J. He et al., "Energy efficient architectures and techniques for green radio access networks," in *Proc. 5th Int. ICST CHINACOM*, Aug. 2010, pp. 1-6, Invited Paper.

[6] Y. Hao, Q. Ni, H. Li and S. Hou, "On the energy and spectral efficiency tradeoff in massive MIMO-enabled HetNets with capacity-constrained backhaul links", *IEEE Trans. Commun.*, vol. 65, no. 11, pp. 4720-4733, Nov. 2017.

[7] X. Ge, J. Yang, H. Gharavi and Y. Sun,"Energy efficiency challenges of 5G small cell networks", *IEEE Commun. Mag.*, vol. 55, no. 5, pp. 184-191, 2017.

[8] S. Samarakoon, M. Bennis, W. Saad, M. Debbah and M. Latva-aho, "Ultra dense small cell networks: Turning density into energy efficiency", *IEEE J. Sel. Areas Commun.*, vol. 34, no. 5, pp. 1267-1280, 2017.

[9] C. Yan, S. Zhang, S. Xu, and G. Y. Li, "Fundamental trade-offs on green wireless networks," *IEEE Commun. Mag.*, vol. 49, no. 6, pp. 30-37, Jun. 2011.

[10] F. Baccelli and B. Blaszczyszyn, "A new phase transition for local delays in MANETs," in *Proc. IEEE INFOCOM*, 2010, pp. 1-9.

[11] M. Haenggi, "The local delay in poisson networks," *IEEE Trans. Inf. Theory*, vol. 59, no. 3, pp. 1788-1802, Mar. 2013.

[12] Y. J. Chun, S. L. Cotton, M. O. Hasnay, and A. Ghrayeb, "Joint optimization of throughput and delay over PPP interfered relay networks," in *Proc. IEEE PIMRC*, 2016, pp. 1-6.

[13] Y. Zhong, W. Zhang and M. Haenggi, "Managing interference correlation through random medium access", *IEEE Trans. Wireless Commun.*, vol. 13, no. 2, pp. 928-941, Feb. 2014.

[14] W. Nie, Y. Zhong, F. Zheng, and W. Zhang, "HetNets with random DTX scheme: Local delay and energy efficiency," *IEEE Trans. Veh. Technol.*, vol. 65, no. 8, pp. 6601-6613, Aug. 2016.

[15] L. Liu, Y. Zhong, W. Zhang, and M. Haenggi, "On the impact of coordination on local delay and energy efficiency in poisson networks," *IEEE Wireless Commun. Lett.*, vol. 4, no. 3, pp. 241-244, Jun. 2015.

[16] M. Haenggi, "Delay scaling in poisson networks," in *Proc. IEEE ISIT*, 2013, pp. 256-260.

[17] Z. Gong, and M. Haenggi, "The local delay in mobile poisson networks," *IEEE Trans. Wireless Commun.*, vol. 12, no. 9, pp. 4766-4777, Sep. 2013.

[18] P. Frenger, P. Moberg, J. Malmodin, Y. Jading, and I. Godor, "Reducing energy consumption in LTE with cell DTX," in *Proc. IEEE VTC Spring*, 2011, pp. 1-5.

[19] K. Hiltunen, "Utilizing eNodeB sleep mode to improve the energyefficiency of dense LTE networks," in *Proc. IEEE PIMRC*, 2013, pp. 3249-3253.

[20] S. Tombaz, S. Han, K. Sung, and J. Zander, "Energy efficient network deployment with cell DTX," *IEEE Commun. Lett.*, vol. 18, no. 6, pp. 977-980, Jun. 2014.

[21] Y. S. Soh, T. Q. S. Quek, M. Kountouris, and H. Shin, "Energy efficient heterogeneous cellular networks," *IEEE J. Sel. Areas Commun.*, vol. 31, no. 5, pp. 840-850, May 2013.

[22] T. Zhang, J. Zhao, L. An and D. Liu, "Energy efficiency of base station deployment in ultra dense HetNets: A stochastic geometry analysis", *IEEE Wireless Commun. Lett.*, vol. 5, no. 2, pp. 184-187, Apr. 2016.

[23] X. Chai, Y. Li, Y. Lv and Z. Zhang, "Joint spectrum-sharing and base-station-sleep model for improving energy efficiency of HetNet," in *Proc. IEEE ICC*, 2015, pp. 1851-1856.

[24] H. Gao, M. Wang and T. Lv, "Energy Efficiency and Spectrum Efficiency Tradeoff in the D2D-Enabled HetNet," *IEEE Trans. Veh. Technol.*, vol. 66, no. 11, pp. 10583-10587, Nov. 2017.

[25] K. M. S. Huq, S. Mumtaz, J. Bachmatiuk, J. Rodriguez, X. Wang and R. L. Aguiar, "Green HetNet CoMP: Energy Efficiency Analysis and Optimization," *IEEE Trans. Veh. Technol.*, vol. 64, no. 10, pp. 4670-4683, Oct. 2015.

[26] C. Saha, M. Afshang and H. S. Dhillon, "Poisson cluster process: Bridging the gap between PPP and 3GPP HetNet models", in *Proc. IEEE ITA*, 2017, pp. 1-9.

[27] M. Afshang, C. Saha, and H. S. Dhillon, "Nearest-neighbor and contact distance distributions for Thomas cluster process," *IEEE Wireless Commun. Lett.*, vol. 6, no. 1, pp. 130-133, Feb. 2017.

[28] R. K. Ganti and M. Haenggi, "Interference and outage in clustered wireless ad hoc networks," *IEEE Trans. Inf. Theory*, vol. 55, no. 9, pp. 4067-4086, Sep. 2009.

[29] V. Suryaprakash, J. Mϕller, and G. Fettweis, "On the modeling and analysis of heterogeneous radio access networks using a Poisson cluster process," *IEEE Trans. Wireless Commun.*, vol. 14, no. 2, pp. 1035-1047, Feb. 2015.

[30] Y. Wang and Q. Zhu, "Modeling and analysis of small cells based on clustered stochastic geometry," *IEEE Commun. Lett.*, vol. 21, no. 3, pp. 576-579, Mar. 2017.

[31] M. Afshang, C. Saha and H. S. Dhillon, "Nearest-neighbor and contact distance distributions for Matern cluster process", *IEEE Commun. Lett.*, vol. 21, no. 12, pp. 2686-2689, Dec., 2017.

[32] Y. J. Chun, M. O. Hasna, and A. Ghrayeb, "Modeling and analysis of HetNet interference using Poisson cluster processes," in *Proc. IEEE PIMRC*, 2014, pp. 681-686.

[33] Y. J. Chun, M. O. Hasna, and A. Ghrayeb, "Modeling heterogeneous cellular networks interference using Poisson cluster processes," *IEEE J. Sel. Areas Commun.*, vol. 33, no. 10, pp. 2182-2195, Oct. 2015.

[34] C. Saha, M. Afshang and H. S. Dhillon, "3GPP-inspired HetNet model using Poisson cluster process: Sum-product functionals and downlink coverage", *IEEE Trans. Commun.*, vol. PP, no. 99, pp. 1-1, 2017.

[35] C. Saha, M. Afshang and H. S. Dhillon, "Enriched K-tier HetNet model to enable the analysis of user-centric small cell deployments", *IEEE Trans. Wireless Commun.*, vol. 16, no. 3, pp. 1593-1608, Mar. 2017.

[36] M. Afshang and H. S. Dhillon, "Poisson cluster process based analysis of HetNets with correlated user and base station locations", *IEEE Trans. Wireless Commun.*, vol. PP, no. 99, pp. 1-1, 2018.

[37] G. Auer et al., "How much energy is needed to run a wireless network?" *IEEE Wireless Commun. Mag.*, vol. 18, no. 5, pp. 40-49, Oct. 2011.

[38] D. Stoyan, W. S. Kendall, and J. Mecke, *Stochastic geometry and its applications*, 2nd ed. Hoboken, NJ, USA: Wiley, 1996.

[39] H. Jo, Y. J. Sang, P. Xia and J. G. Andrews, "Heterogeneous Cellular Networks with Flexible Cell Association: A Comprehensive Downlink SINR Analysis," *IEEE Trans. Wireless Commun.*, vol. 11, no. 10, pp. 3484-3495, Oct. 2012.

[40] K. Li, C. Yang, Z. Chen and M. Tao, "Optimization and Analysis of Probabilistic Caching in N -Tier Heterogeneous Networks," *IEEE Trans. Wireless Commun.*, vol. 17, no. 2, pp. 1283-1297, Feb. 2018.

[41] S. Lee and K. Huang, "Coverage and Economy of Cellular Networks with Many Base Stations," *IEEE Commun. Lett.*, vol. 16, no. 7, pp. 1038-1040, July 2012.

Xiaojie Dong received the B.S. in Electronic Information Engineering from Heilongjiang University, China in 2016 and the MEng in Information and Communication Engineering from Harbin Institute of Technology, Shenzhen, China in 2019. His research interests include Stochastic geometry and Heterogeneous networks.

Fu-Chun Zheng obtained the BEng (1985) and MEng (1988) degrees in radio engineering from Harbin Institute of Technology, China, and the PhD degree in Electrical Engineering from the University of Edinburgh, UK, in 1992.

From 1992 to 1995, he was a post-doctoral research associate with the University of Bradford, UK, Between May 1995 and August 2007, he was with Victoria University, Melbourne, Australia, first as a lecturer and then as an associate professor in mobile communications. He was with the University of Reading, UK, from September 2007 to July 2016 as a Professor (Chair) of Signal Processing. He has also been a distinguished adjunct professor with Southeast University, China, since 2010. Since August 2016, he has been a distinguished professor with Harbin Institute of Technology (Shenzhen), China and the University of York, UK. He has been awarded two UK EPSRC Visiting Fellowships - both hosted by the University of York (UK): first in August 2002 and then again in August 2006. Over the past two decades, Dr Zheng has also carried out many government and industry sponsored research projects - in Australia, the UK, and China. He has been both a short term visiting fellow and a long term visiting research fellow with British Telecom, UK. Dr Zheng's current research interests include signal processing for communications, multiple antenna systems, green communications, and ultra-dense networks.

He was an editor (2001-2004) of IEEE Transactions on Wireless Communications. In 2006, Dr Zheng served as the general chair of IEEE VTC 2006-S, Melbourne, Australia (www.ieeevtc.org/vtc2006spring) - the first ever VTC held in the southern hemisphere in VTC's history of six decades. More recently he was the executive TPC Chair for VTC 2016-S, Nanjing, China (the first ever VTC held in mainland China: www.ieeevtc.org/vtc2016spring).

Xu Zhu (S'02-M'03-SM'12) received the B.Eng. degree (with the first-class Hons.) in electronics and information engineering from Huazhong University of Science and Technology, Wuhan, China, in 1999, and the Ph.D. degree in electrical and electronic engineering from the Hong Kong University of Science and Technology, Hong Kong, in 2003. She joined the Department of Electrical Engineering and Electronics, the University of Liverpool, Liverpool, U.K. in 2003 as an academic member, where she is currently a Reader. She has over 160 peer-reviewed publications on communications and signal processing. Her research interests include MIMO, channel estimation and equalization, resource allocation, cooperative communications, green communications, etc. She has acted as a chair for various international conferences, such as Symposium Co-Chair of IEEE ICC 2016 and 2019, Vice-Chair of the 2006 and 2008 ICARN International Workshops, Program Chair of ICSAI 2012, and Publicity Chair of IEEE IUCC-2016. She has served as an Editor for the IEEE TRANSACTIONS ON WIRELESS COMMUNICATIONS and a Guest Editor for several international journals such as Electronics.

Timothy O'Farrell is a Chair Professor in Wireless Communications at the University of Sheffield, UK. He is an expert in wireless communication systems specialising in physical layer signal processing, radio resource management and wireless network planning. He has pioneered research on energy efficient mobile cellular communications, the mathematical modeling of CSMA based MAC protocols for WiFi, iterative block coding for wireless communication systems and spreading sequence design for CDMA wireless networks. He is an entrepreneur, being the cofounder and CTO of Supergold Communication Limited (1997-2007), a start-up that participated in the standardisation of IEEE 802.11g with the M-BCK proposal. In the framework of Mobile VCE (mVCE), Professor O'Farrell was the Academic Coordinator of the Core 5 Green Radio project (2009-2012) and a leader in establishing energy efficiency as a global research field in wireless communications systems. He has managed 23 major research projects as principal investigator. His current EPSRC project portfolio as PI includes the SERAN, FARAD and DDmmMaMi projects. He has published 313 journal & conference papers, book chapters, patents and technical reports; and has participated in standards, consultancy and expert witness activities within the wireless sector. Currently, Professor O'Farrell is leading the UK Research Strategy Community Organisation in Communications, Mobile Computing and Networking within the EPSRC portfolio (www.commnet.ac.uk). Professor O'Farrell is a Director of the mVCE, a Chartered Engineer, an IET member and an IEEE senior member.